minerals

MDPI

Article

The Cedrolina Chromitite, Goiás State, Brazil: A Metamorphic Puzzle

Yuri de Melo Portella [1,*], Federica Zaccarini [2], George L. Luvizotto [1], Giorgio Garuti [2], Ronald J. Bakker [2], Nelson Angeli [1] and Oskar Thalhammer [2]

[1] Department of Petrology and Metallogeny, São Paulo State University (UNESP), 24-A Avenue, 1515, Rio Claro (SP) 13506-900, Brazil; george.luvizotto@gmail.com (G.L.L.); nangeli@rc.unesp.br (N.A.)

[2] Department of Applied Geological Sciences and Geophysics, University of Leoben, Peter Tunner Str. 5, A-8700 Leoben, Austria; federica.zaccarini@unileoben.ac.at (F.Z.); giorgiogaruti1945@gmail.com (G.G.); ronald.bakker@unileoben.ac.at (R.J.B.); oskar.thalhammer@unileoben.ac.at (O.T.)

* Correspondence: yuri_portella@hotmail.com; Tel.: +55-199-910-80987

Academic Editor: Paul Sylvester
Received: 1 July 2016; Accepted: 25 August 2016; Published: 1 September 2016

Abstract: The Cedrolina chromitite body (Goiás-Brazil) is concordantly emplaced within talc-chlorite schists that correspond to the poly-metamorphic product of ultramafic rocks inserted in the Pilar de Goiás Greenstone Belt (Central Brazil). The chromite ore displays a nodular structure consisting of rounded and ellipsoidal orbs (up to 1.5 cm in size), often strongly deformed and fractured, immersed in a matrix of silicates (mainly chlorite and talc). Chromite is characterized by high Cr# (0.80–0.86), high Fe^{2+}# (0.70–0.94), and low TiO_2 (av. = 0.18 wt %) consistent with variation trends of spinels from metamorphic rocks. The chromitite contains a large suite of accessory phases, but only irarsite and laurite are believed to be relicts of the original igneous assemblage, whereas most accessory minerals are thought to be related to hydrothermal fluids that emanated from a nearby felsic intrusion, metamorphism and weathering. Rutile is one of the most abundant accessory minerals described, showing an unusually high Cr_2O_3 content (up to 39,200 ppm of Cr) and commonly forming large anhedral grains (>100 μm) that fill fractures (within chromite nodules and in the matrix) or contain micro-inclusions of chromite. Using a trace element geothermometer, the rutile crystallization temperature is estimated at 550–600 °C (at 0.4–0.6 GPa), which is in agreement with P and T conditions proposed for the regional greenschist to low amphibolite facies metamorphic peak of the area. Textural, morphological, and compositional evidence confirm that rutile did not crystallize at high temperatures simultaneously with the host chromitite, but as a secondary metamorphic mineral. Rutile may have been formed as a metamorphic overgrowth product following deformation and regional metamorphic events, filling fractures and incorporating chromite fragments. High Cr contents in rutile very likely are due to Cr remobilization from Cr-spinel during metamorphism and suggest that Ti was remobilized to form rutile. This would imply that the magmatic composition of chromite had originally higher Ti content, pointing to a stratiform origin. Another possible interpretation is that the Ti-enrichment was caused by external metasomatic fluids which lead to crystallization of rutile. If this was the case, the Cedrolina chromitites could be classified as podiform, possibly representing a sliver of tectonically dismembered Paleoproterozoic upper mantle. However, the strong metamorphic overprint that affected the studied chromitites makes it extremely difficult to establish which of the above processes were active, if not both (and to what extent), and, therefore, the chromitite's original geodynamic setting.

Keywords: chromitite; accessory minerals; rutile; metamorphism; Pilar de Goiás; greenstone belt; Brazil

1. Introduction

The Cedrolina chromitite occurs in the Pilar de Goiás Greenstone Belt (Brazil) and is associated with mica-schist, amphibolite, amphibole-schist and banded iron formation rich in magnetite and amphibole of the Cedrolina formation. These rocks represent the poly-metamorphic products of mafic–ultramafic rocks and associated sedimentary deposits. The Cedrolina chromitite was explored for noble metals by mining companies in the late 1980s. However, probably due to its small size (230 × 100 m), the mineralized body was never exploited and little is known about its mineralogical and petrological aspects. Thus, the study of the Cedrolina chromitite provides a useful example to understand the evolution of chromite composition from the magmatic stage, through a long metamorphic history and also after lateritic weathering. Attempting to comprehend this evolution is not a simple task, and accessory phases can play an important role in clarifying which kinds of metamorphic processes affected the studied rocks, their thermodynamic conditions, and insights on the possible protolith composition.

Although accessory minerals occur in small quantities in their host rocks, a number of them can be used to obtain precise geochronological data, as well as to model the physico-chemical conditions of their crystallization. Furthermore, accessory minerals can also provide useful information about the type of magma and/or type of fluid from which they precipitate [1]. The platinum group minerals (PGM), with few exceptions, are grouped among accessory phases, being rare and occurring as tiny particles dispersed in their host rocks. Recent investigations have shown that the primary/magmatic PGM may be altered to secondary PGM during metamorphism, as well as weathering and lateritization [2–12]. It has also been demonstrated that hydrothermal solutions and metamorphic fluids are capable of introducing incompatible elements in the alteration system of a chromitite, giving rise to the formation of exotic accessory minerals, such as monazite, galena, bismuthinite, and antimony that normally do not occur in unaltered chromitites [13,14]. In a number of contributions [15–18] it has been shown that certain trace elements can be successfully used to evaluate the crystallization temperature of rutile, as well as the behavior of the mineral under different metamorphic reactions. Likewise, trace element concentrations in zircon can be used to identify its geochemical signature and, therefore, probable source rock. Average rare earth element (REE) concentration in zircons from mafic rocks range from several hundred to 1000 ppm (rarely over 2000 ppm), reaching per cent levels in granitoids/pegmatites. Titanium concentrations, however, commonly are below 6 ppm especially in zircons from kimberlites and mafic rocks, reaching 500–700 ppm in granites [19]. The presence of monazite in the Cedrolina chromitite was documented in a previous paper [14] and the authors suggested that this mineral did not crystallize at high temperature in equilibrium with the host chromitite, but formed during one of the metamorphic events that affected the area.

In this contribution we report, for the first time, the results of a detailed mineralogical study of the Cedrolina chromitite, with special regard to: (i) the composition and texture of the chromite; (ii) assemblage, mineralogical nature and petrological significance of the accessory phases; and (iii) trace element distribution and geothermic calculations of rutile. The obtained data are used to discuss the genetic aspects of the Cedrolina chromitite, the effects produced by metamorphism on chromite composition, and also to estimate the local metamorphic peak temperature. The role of the accessory minerals as petrogenetic indicators is also evaluated and confirmed.

2. Geological Background and Description of the Investigated Chromitite

The Cedrolina chromitite is located about 300 km northwest of Brasília, in the State of Goiás (Figure 1A–C). It consists of a tabular, elliptical body of 230 × 100 m, striking NE-SW, with thicknesses varying from 1 to 2.4 m and hosted by talc-chlorite-schist (Figure 1D) [20]. All rocks of the studied area have been thoroughly altered by tropical weathering conditions and the area displays deep soil profiles and extensive lateritic covers (rich in manganese and iron oxides/hydroxides). Outcrops are very rare and geological mapping is rather challenging, frequently relying on soil and float blocks (samples 12,

14, 100, and 106). Relatively fresh chromitite outcrops (samples 47 and 105) occur only along a roadside cut, making it difficult to collect enough structural data for such a deformed area. Nonetheless, the chromitite displays a discrete to prominent schistosity, highlighted by the oriented silicates of the matrix (talc + chlorite), dipping 20° to the NW, concordant with the regional foliation of the country rocks (20°–50° to the NW) [20]. Samples 14, 47, 105, and 106 are from the main chromitite body, whereas sample 100 is a float block that was collected ~300 m South (closest to the felsic intrusion).

The general geological setting of the area consists of greenschist [21] to amphibolite facies [22] metavolcanosedimentary sequence of the Pilar de Goiás greenstone belt. The greenstone belt is in contact to the West with the ~2.71 Ga Moquém Block and to the East with the 2.85 Ga Hidrolina Complex, both composed of granite and gneiss (simplified after [23], Figure 1C). The northern Goiás State supracrustal rocks that comprise the Crixás, Guarinos, and Pilar de Goiás greenstone belts, were all affected by similar regional metamorphic conditions [24]. According to [21,25,26] the regional metamorphic conditions of the Crixás Belt vary from greenschist to low amphibolite facies. Although there is no consensus on the number of tectono-metamorphic events and their specific ages, four deformational stages have been suggested in the literature [26], two during the Paleoproterozoic (including the main metamorphic event) and two in the Neoproterozoic.

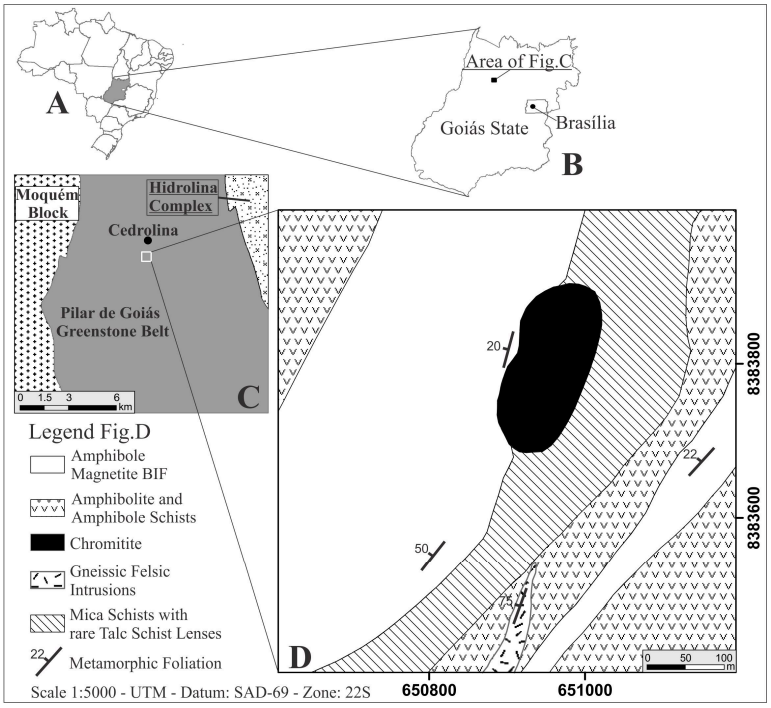

Figure 1. Geological sketch maps of Cedrolina chromitites (**A**,**B**)—Geographical location of the studied area; (**C**)—General geology of the central-northern Pilar de Goiás greenstone belt area simplified after [23]; (**D**)—Detailed geological map of a small portion of the Cedrolina Formation where the investigated chromitites occur [20].

The stratigraphy of the Pilar de Goiás greenstone belt is divided into two main sequences [27]: the lower one (to the East) that consists of mafic–ultramafic metavolcanic rocks with minor intercalated metasedimentary thin beds and lenses (Córrego Fundo Formation—metakomatiites; Cedrolina Formation—metabasalts), and the upper one (to the West) that is formed by metasediments (Boqueirão Formation—metacherts, calcsilicates and marbles; Serra do Moínho Formation—metapelites).

The Cedrolina chromitite occurs within the lower mafic–ultramafic metavolcanic rocks of the Cedrolina Formation, and is hosted by talc-chlorite schist. The contact between the chromitite and the talc-chlorite schist was not observed in situ due to the intense deformation, weathering and reduced

number of outcrops. However, in some blocks sharp to graded contacts are still visible. The body is in contact with mica-schists to the East and banded iron formations (BIF) rich in cummingtonite-grunerite and magnetite to the West (Figure 1D). Amphibolites and amphibole schists of the Cedrolina Formation mapped in the Cedrolina area [20] are composed mainly of hornblende, cummingtonite-grunerite, andesine, garnet, ±magnetite and ±titanite (devoid of chlorite and clinopyroxene) which is a typical paragenesis of mafic rocks metamorphosed under amphibolite facies conditions (T > 570 °C and pressures of 0.4–0.6 GPa, Figure 2 modified after [28]). The same author also recognized impure marbles of the Boqueirão Formation composed of calcite, tremolite, and quartz, as well as BIF (of the Cedrolina Formation) rich in cummingtonite-grunerite and magnetite, corroborating a greenschist to amphibolite facies metamorphism over metasedimentary rocks in the Cedrolina area. In the mafic schists of the Cedrolina Formation, hornblende and andesine are partially to almost completely transformed into tremolite and epidote, respectively, cummingtonite is often transformed to chlorite and chlorite into talc (in talc-schists), which attests a retrograde metamorphism of the greenschist facies [20].

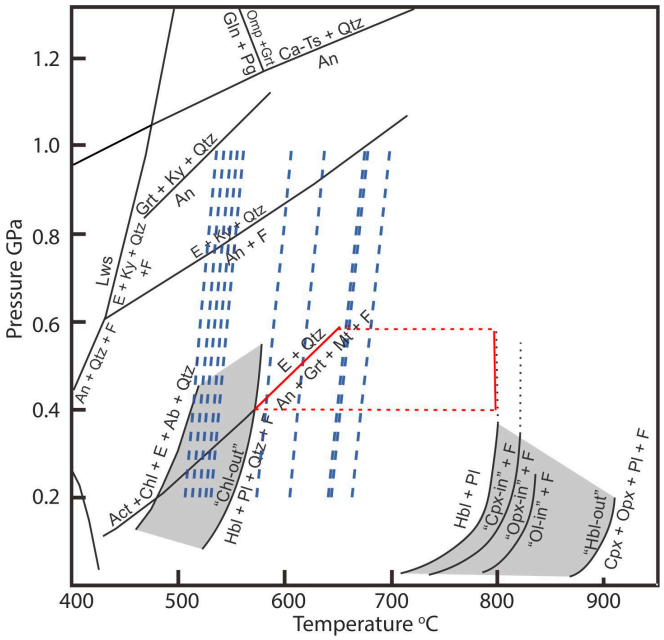

Figure 2. Simplified petrogenetic grid for metamorphosed mafic rocks modified after [28]. The red polygon represents the paragenesis hornblende, garnet, andesine, and magnetite (devoid of chlorite and clinopyroxene) described by [20] in amphibolites and amphibole schists of the Cedrolina Formation indicative of T > 570 °C and Pressures of 0.4–0.6 GPa. Dashed blue lines represent temperatures calculated using the Zr-in-rutile geothermometer for crystals in samples 14, 100, 105, and 106 (for details about the temperature calculations and dataset please refer to the text). Notice that the pressure effect for the 0.2–1.0 GPa range is less than 35 °C. Mineral abbreviations (Ab = albite, Act = actinolite, An = anorthite, Ca-Ts = Ca-tschermakite, Chl = chlorite, Cpx = Ca-clinopyroxene, *E* = an epidote mineral: epidote, zoisite, or clinozoisite, *F* = aqueous fluid, Gln = glaucophane, Grt = garnet, Hbl = hornblende, Ky = kyanite, Lws = lawsonite, Mt = magnetite, Ol = olivine, Omp = omphacite, Opx = orthopyroxene, Pg = paragonite, Pl = plagioclase, Qtz = quartz).

It has been suggested that the granite-greenstone belt association of central Brazil could represent an Archean crustal segment and, as a consequence, the supracrustal rocks of northern Goiás State (greenstone belts of Crixás, Guarinos and Pilar de Goiás) were also considered to be Archean in age [29]. However, Paleoproterozoic ages have been proposed for the sedimentary sequences of the greenstone belts of central Brazil [25,30,31]. Sm–Nd whole rock analyses were carried out for a basal metachert and three calcsilicate rocks from different stratigraphic positions of the Boqueirão Formation

of the Pilar de Goiás greenstone belt [31]. The analyzed samples yielded a Sm–Nd isochron date of 2189 ± 36 Ma suggesting a Paleoproterozoic age. According to the same authors, despite the expected error of the Sm–Nd isotopic determinations, it is plausible to estimate that the formation age of these chemical deposits is roughly 2.2 Ga. The age of the lower mafic–ultramafic metavolcanic sequences is still matter of debate, and hence, the age of those units could be either Archean or Paleoproterozoic.

Small bodies of albite gneisses occur within the greenstone belts of northern Goiás. These rocks are interpreted as granitic intrusions [24] and are composed of albite and quartz, rare microcline, and accessory phases are biotite, amphibole, zircon, apatite, pyrite, magnetite, and ilmenite. U–Pb SHRIMP data on zircons from an albite granite-gneiss that occurs in the Pilar de Goiás greenstone belt yielded concordant ages of about 2145 Ma [24].

3. Analytical Techniques

Electron microprobe analyses were carried out at the Eugen F. Stumpfl laboratory (Leoben University, Leoben, Austria), using a Jeol JXA 8200 Superprobe (Peabody, MA, USA) with the most adequate conditions for each type of mineral. Wavelength dispersive spectrometer (WDS) and energy dispersive spectrometer (EDS) modes were used for quantitative and qualitative analyses, respectively. The same instrument was used to obtain electronic images. Chromite and silicates were quantitatively analyzed with 15 kV of accelerating voltage and 10 nA of beam current. All the elements were analyzed using the Kα line, and were calibrated on natural chromite, rhodhonite, ilmenite, wollastonite, kaersutite, olivine, millerite, and metallic V. The following diffracting crystals were used: TAP for Mg, Al and Na, PETJ for Si, K and Ca, and LIFH for Ti, V, Cr, Mn, Ni, and Fe. The counting times for peak and background were 20 and 10 s respectively. The amount of Fe^{3+} in chromite was calculated assuming spinel stoichiometry. Most of the accessory minerals were only qualitatively analyzed by EDS, owing to their small size (less than 5 micrometers). Only the alloys composed of Au, Pd, Cu and Ni were quantitatively analyzed using 20 kV of accelerating voltage and 10 nA of beam current and with 20 and 10 s of counting time for peak and background, respectively. The following analyzing crystals were selected: PETH for Pd and Au and LIFH for Cu and Ni. Kα line was used for Cu and Ni, Lα line for Pd and Mα line for Au. Pd was calibrated on native palladium, Au on electrum, Cu on chalcopyrite, and Ni on millerite. Rutile and zircon were quantitatively analyzed with 20 kV of accelerating voltage and 30 nA of beam current. The counting times were increased up to 60 and 30 s for peak and background, respectively. Kα line was used for Mg, Cr, Ti, Al, Mn, Fe, Si, Hf, and V and Lα line for Nb, Zr, Y, Ce, La, Nd, Pr, and W and Mα line for U, Th, and Pb. The following standards were selected: natural olivine, chromite, albite, rutile, rhodonite, magnetite and zircon, galena, synthetic metallic Nb, V, Th, U, and W, synthetic Y-garnet and rare earth element (REE) glass. The TAP crystal was used for Mg and Al, the PETH for Si, Y, U, Th, and Pb, the PETJ for Nb, Mn, and Zr, the LIFH for Cr, Ti, W, Fe, V, Ce, La, Nd, Pr, and Hf. Since in the rutile and zircon most of the analyzed elements occur as trace and ultra-trace, with the selected conditions the following detection limits, in ppm, were achieved: Mg, Al, V and Fe = 30, Nb = 110, Cr = 45, Ti = 105, Mn = 100, W = 135, Zr = 55, Si = 105, Hf = 130, Y = 140, U = 60, Th = 20, Pb = 70, Ce = 200, La = 500, Nd = 800 and Pr = 550. The detection limits were automatically calculated by Jeol software taking into consideration (1) average X-ray intensity of background; (2) counting time of the background signal; (3) intensity of the characteristic X-ray of the analyzed element; and (4) mass concentration in the standard sample. The quantification of trace and ultra-trace elements by electron microprobe may cause analytical uncertainties. However, the precision and accuracy of Zr measurements in rutile and trace elements measured in zircon were evaluated by additional analyses performed on a rutile standard, containing 1 wt % of Zr_2O_3, available to one of the authors (GG) and on synthetic glasses and natural zircon standards, available at the Eugen F. Stumpfl laboratory. Rutile was also investigated by Raman spectroscopy, to distinguish it from its polymorphs, anatase and brookite, as suggested by [32]. Raman spectra were collected using a LABRAM (ISA Jobin Yvon, Albuquerque, NM, USA), instrument at the University of Leoben. A frequency-doubled 100 mW Nd-YAG laser with an excitation wavelength of λ = 532.6 nm was

used. The polarization state of the laser is consistent with the north-south direction (*y*-axis) of the microscope stage. Measurements were carried out with an LMPlanFI 100×/0.8 (Olympus, Tokyo, Japan) objective lens and they have an accuracy of 1.62 cm^{-1} at low Δv (about 0 cm^{-1}) and of 1.1 cm^{-1} at high Δv (about 3000 cm^{-1}). The following standards were employed for internal calibration: silicon (520 cm^{-1}), polyethylene (1062, 1128, 1169, 1295, 1487, 1439, 2848, 2881 cm^{-1}), calcite (156, 283, 713, 1087, 1437 cm^{-1}) and diamond (1332 cm^{-1}).

4. Mineral Descriptions and Compositions

4.1. Chromitite and Chromite

The chromitite modal composition is characterized by 40%–70% of chromite (av. 60%), 14%–55% of talc (av. 25%), 3%–60% Cr-rich chlorite (av. ~15%), traces up to 4% of iron hydroxides (av. ~0.7%) and traces up to 2% of rutile (av. ~0.5%) and, therefore, is classified as disseminated. Macroscopically the chromitite ore is characterized by a peculiar nodular structure, consisting of rounded nodules (0.5–1.5 cm in diameter, av. 1 cm) associated with a matrix of silicates (mainly Cr-rich chlorite and talc) and minute chromite fragments (Figure 3A–E). This structure resembles those of mantle hosted ophiolitic chromitite from Troodos-Cyprus (Figure 3F). Both chromite and the matrix silicates present moderate (Figure 3C) to high (Figure 3E) weathering stages. The chlorite in the matrix contains high Cr_2O_3 (av. > 3.0 wt %—Table 1) and is partially or almost completely converted into talc. Nonetheless, both minerals are interpreted to be secondary metamorphic products of the primary magmatic silicates.

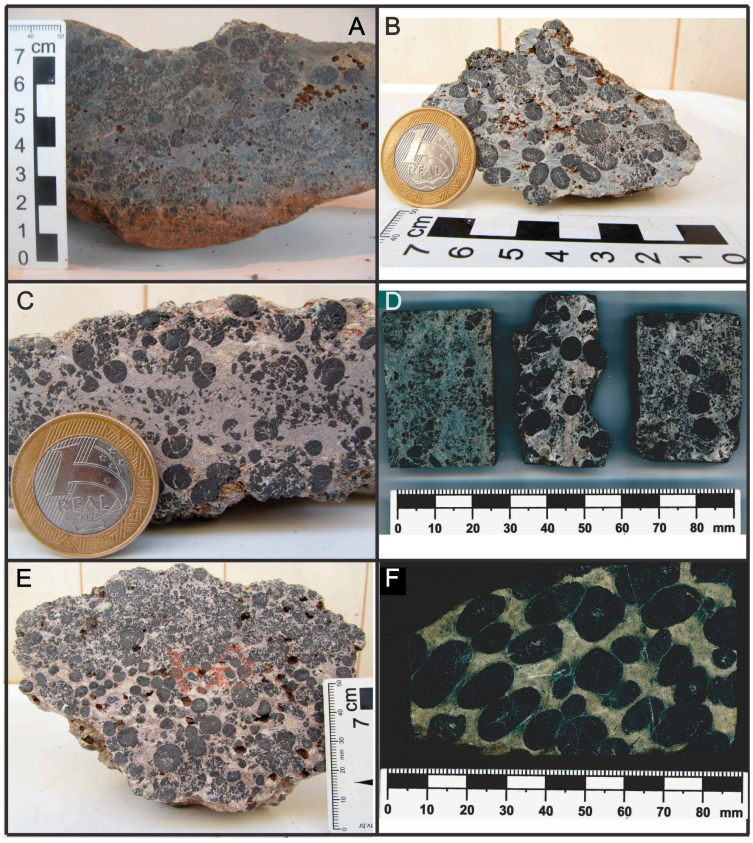

Figure 3. Hand specimens of the Cedrolina chromitite. (**A**) Slightly altered dark green chromitite (sample 106A); (**B**) Initial stage of weathering showing bluish green color of the matrix silicates (sample 100); (**C**) Moderate weathering exhibiting grayish color (sample 105C); (**D**) Spherical chromite nodules and minute chromite particles dispersed in the silicate matrix; (**E**) Intensely weathered rock with whitish-pinkish colored matrix (sample 47B); (**F**) Hand specimen of a mantle hosted ophiolitic chromitite from Troodos (Cyprus) evidencing nodular "leopard" chromite with coalescent contacts.

Table 1. Selection of representative electron microprobe analyses of chlorite from Cedrolina chromitite (wt %).

Sample CED	SiO_2	Al_2O_3	MgO	FeO	Cr_2O_3	Total
47A	32.92	14.18	32.36	1.89	3.78	85.13
47A	33.34	13.76	33.02	2.23	4.20	86.55
47A	31.57	16.03	31.88	2.41	4.25	86.14
47A	33.09	13.71	33.03	2.01	3.93	85.78
47A	32.77	13.91	32.90	1.80	3.99	85.36
47A	30.93	16.53	31.21	2.31	3.85	84.83
47A	32.92	14.57	32.47	1.99	4.03	85.97
47A	29.92	17.66	30.85	2.24	4.17	84.84
105C	29.52	17.06	31.21	2.26	3.30	83.35
105C	28.62	18.87	30.22	2.30	3.40	83.41
105C	29.25	18.03	29.40	2.54	3.96	83.18
105C	30.02	15.98	30.90	2.17	3.95	83.02
105C	30.26	16.29	31.87	2.11	3.62	84.14
106D	31.70	17.60	27.99	4.10	2.13	83.52
106D	32.10	17.92	29.25	3.94	1.99	85.21
106D	32.06	19.22	28.19	3.51	2.19	85.17
106D	29.86	20.30	27.43	4.02	2.47	84.09
106D	31.15	17.35	29.79	3.78	2.10	84.17

Rare grains of phlogopite, amphiboles, and clinopyroxene occur as small inclusions in chromite. Clinopyroxene may represent the only relict of the original igneous silicates. Magnetite, Al-Mg hydroxides, carbonates, phosphates (commonly hydrated), and barite occur in the silicate matrix as minor phases. Microscopically, the chromite displays a very complex and puzzling nodular texture as shown in Figure 4. The nodules consist of massive chromite (Figure 4A), which are often fractured. The fractures are mostly filled with chlorite (Figure 4B–D) and rarely with rutile. The image presented in Figure 4D shows the internal structure of a nodule that is characterized by the presence of euhedral crystals of chromite with very sharp/linear contacts and triple junctions among themselves. Single large crystals of chromite also occur (Figure 4E) as well as euhedral chromite grains of various sizes (Figure 4F). The grains in Figure 4D,F, particularly, show hexagonal and octahedral shapes, typical of the isometric crystallographic system of spinels. Recrystallization played a role in fading some of the polygonal contacts, but some distinctively sharp edges are still visible.

More than 500 electron microprobe analyses were performed on 15 samples and a selection of representative analyses is listed in Table 2. The composition of chromite is not homogeneous, with Cr_2O_3 and Al_2O_3 contents comprised between 41.93–63.45 wt % and 2.76–11.10 wt %, respectively. MgO varies from 0.47 up to 8.71 wt % and FeO from 19.45 up to 31.93 wt %. Fe_2O_3 ranges from 0.68 up to 21.80 wt %. Among the trace elements, the Cedrolina chromite exhibits systematically high values of MnO (0.51–1.14 wt %) and low values of V_2O_3 (<0.27 wt %). NiO is below detection limit and TiO_2 is characterized by a wide spread from below the electron probe micro-analyzer (EPMA) detection limit to 1.36 wt %.

Observed compositional variations are not related with distinct chromite forms of occurrence (e.g., massive nodules, large or small euhedral crystals). Furthermore, no compositional zoning within a single grain/nodule was recognized (e.g., magnetite/ferrian chromite rims) using microprobe analyses. In the binary TiO_2 versus Cr_2O_3 diagram [33,34] of Figure 5A, most compositions plot in the field of the podiform chromitite associated with the ophiolitic mantle. Few data plot in the field of the stratiform chromitite occurring in the layered complexes and some analyses are remarkable for their high TiO_2 and Cr_2O_3 values (Figure 5A). Considering Cr# and Mg#, the Cedrolina chromite composition plots outside the fields of both podiform and stratiform chromitites, since they are characterized by high values of Cr# and low Mg# [33,34] (Figure 5B). They also differ from the Neoproterozoic podiform chromitites of Egypt and Saudi Arabia which are characterized by a large

variation of Cr# and low Mg# [35–38]. Compared with the Cr–Al–Fe^{3+} compositions of spinels from different metamorphic facies [39–41] (Figure 6A), as well as with spinel stability limits [42,43] (Figure 6B), most of the Cedrolina chromite is comprised in the field of spinel metamorphosed in the upper greenschist facies, at temperatures ranging from 500 to 550 °C (Figure 6B).

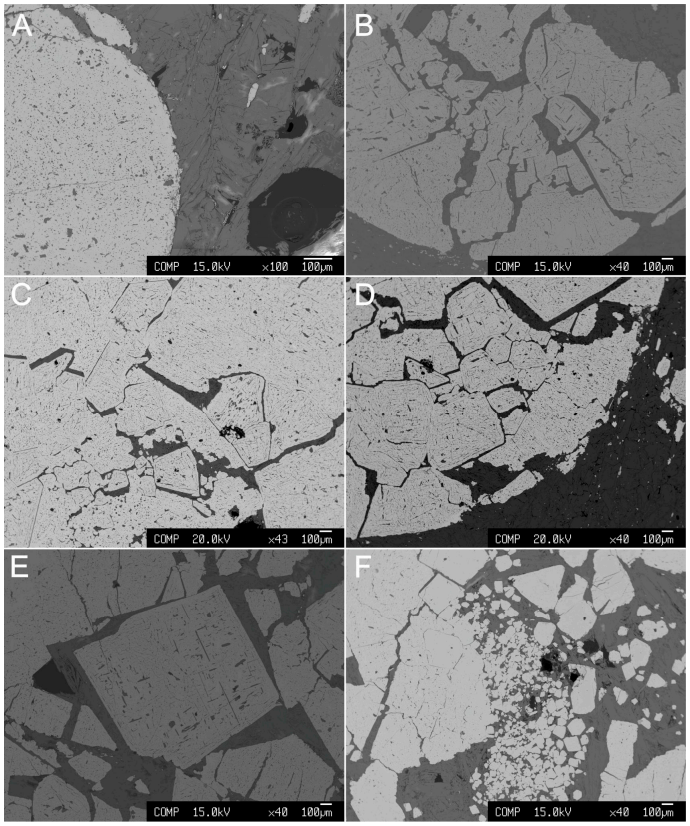

Figure 4. Backscattered electron images (BSE) of the Cedrolina chromitite. (**A**) Massive chromite nodule; (**B**) Fractured chromite nodule; (**C**,**D**) Internal texture of the nodules characterized by the presence of euhedral crystals of chromite with very sharp/linear contacts amongst themselves. Fractures superimpose former sharp contacts, resembling a cumulus-type texture; (**E**) Single large crystal of chromite; (**F**) Various sizes of euhedral chromite crystals.

Table 2. Selection of representative electron microprobe analyses of chromite from Cedrolina chromitite (wt %). Bd—below the detection limit.

Sample CED	Al_2O_3	Fe_2O_3	Cr_2O_3	FeO	MgO	MnO	TiO_2	V_2O_3	Total
100	8.1	9.7	49.51	29.83	1.89	0.78	0.25	0.16	100.22
100	6.66	11.03	49.89	30.47	1.58	0.76	0.41	0.17	100.97
100	5.78	12.45	50.2	30.17	1.48	0.92	0.15	0.16	101.31
100	7.79	10.83	49.15	30.28	1.75	0.77	0.3	0.12	101
105A	5.48	3.25	59.16	27.22	3.2	0.66	0.06	0.16	99.18
105A	10.05	3.24	55.15	27.43	3.89	0.56	0.1	0.19	100.6
105A	5.82	3.04	60.1	27.42	3.37	0.64	0.05	0.18	100.6
105A	6.56	3.75	58.24	27.03	3.64	0.62	0.02	0.11	99.97
105A	10.16	0.68	55.56	28.29	3.95	0.52	1.1	0.23	100.48
105B	8.66	5.57	54	25.64	4.55	0.67	0.12	0.19	99.39
105B	7.57	4.85	55.58	26.61	4.37	0.62	0.65	0.17	100.43
105B	4.44	4.38	60.81	26.79	3.64	0.67	0.02	0.19	100.93
105B	5.53	4.62	59.67	25.96	4.28	0.63	bd	0.12	100.82
105C	5.81	2.5	60.75	25.12	4.74	0.67	0.03	0.11	99.73
105C	9.15	2.51	57.56	24.33	5.82	0.51	0.17	0.16	100.23

Table 2. *Cont.*

Sample CED	Al_2O_3	Fe_2O_3	Cr_2O_3	FeO	MgO	MnO	TiO_2	V_2O_3	Total
105C	4.08	1.99	63.45	25.74	4.31	0.66	0.06	0.03	100.32
105C	11.1	2.02	55.79	24.53	5.95	0.55	0.15	0.27	100.36
106A1	3.55	21.8	41.93	31.93	0.47	0.61	0.64	0.15	101.1
106A1	5.23	11.07	51.31	31.15	0.83	0.65	0.13	0.02	100.39
106A1	7.58	10.96	49.04	31.69	0.86	0.67	0.12	0.14	101.08
106A1	9.18	9.75	48.28	31.57	1.09	0.66	0.2	0.19	100.91
106A2	2.76	21.42	42.64	31.3	0.54	0.59	0.57	0.15	99.99
106A2	7.2	11.14	49.3	31.18	1	0.68	0.13	0.11	100.73
106A2	8.5	9.39	48.74	31.33	1.11	0.6	0.28	0.22	100.16
106A2	9.44	8.77	49.24	31.13	1.37	0.58	0.11	0.18	100.81
106B	4.94	6.09	57.77	27.31	3.05	0.93	0.07	0.1	100.25
106B	6.31	6.58	55.25	26.92	3.29	0.91	0.07	0.12	99.45
106B	6.97	6.3	54.01	27.11	3.41	0.86	0.42	0.11	99.17
106B	8.26	6.77	53.06	26.52	3.8	0.81	0.06	0.14	99.43
106C	4.21	6.62	57.57	27.59	2.62	0.96	0.02	0.11	99.7
106C	7.36	5.88	52.33	28.7	3.12	0.82	1.36	0.16	99.74
106C	7.93	7.29	52.95	27.43	3.32	0.84	0.12	0.17	100.05
106C	8.46	6.87	52.63	27.15	3.44	0.8	0.07	0.12	99.56
106D	5.98	6.65	55.76	29.22	1.98	1.05	0.06	0.14	100.84
106D	7.89	6.79	53.3	28.93	2.21	1.14	0.08	0.15	100.48
106D	8.39	6.1	52.17	29.23	2.38	1	0.6	0.13	99.99
106D	10.01	7.13	50.51	29.2	2.47	0.98	0.17	0.17	100.63
106E	5.45	7.05	55.76	27.92	2.69	0.89	0.12	0.03	99.91
106E	6.54	8.5	52.8	27.92	2.77	0.96	0.2	0.2	99.88
106E	7.05	8.2	52.69	27.66	3	0.97	0.21	0.09	99.87
106E	7.86	7.83	51.69	27.58	3.11	0.81	0.22	0.1	99.21
12	5.15	4.44	59.6	23.59	5.43	0.73	0.09	0.14	99.18
12	6.99	5.07	57.17	23.55	5.87	0.71	0.25	0.14	99.75
12	8.61	5.7	54.64	23.07	6.12	0.81	0.12	0.26	99.32
12	10.19	7.01	52.84	19.45	8.71	0.61	0.12	0.11	99.04
47A	7.21	2.91	59.33	25.32	4.81	0.77	0.05	0.15	100.55
47A	7.91	3.81	57.65	25.42	4.82	0.76	0.07	0.12	100.55
47A	9.57	4.19	55.49	25.44	5.02	0.71	0.09	0.18	100.68
47A	10.13	3.94	55.11	25.28	5.22	0.6	0.08	0.2	100.56
47B	5.69	4.41	60.09	24.38	5.31	0.64	0.01	0.18	100.73
47B	6.14	4.66	59.4	24.21	5.44	0.76	0.05	0.2	100.86
47B	7.78	5.51	56.53	24.15	5.71	0.71	0.17	0.15	100.7
47B	8.91	6.21	54.71	23.52	6.21	0.63	0.12	0.16	100.47
47C	9.8	8.6	51.08	20.14	8.71	0.63	0.74	0.12	99.81
47C	7.84	6.24	55.15	23.77	5.73	0.67	0.11	0.15	99.67
47C	8.18	6.55	54.7	23.45	5.96	0.76	0.12	0.1	99.81
47C	9.01	6.87	53.68	23.46	6.07	0.72	0.07	0.15	100.04

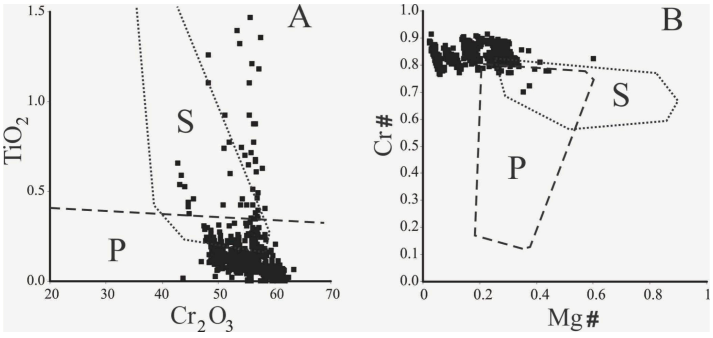

Figure 5. Binary diagrams showing podiform (P) and stratiform (S) chromite fields where >500 chromite analyses from Cedrolina were plotted (modified after [33,34]). (**A**) TiO_2 vs. Cr_2O_3; (**B**) Cr# vs. Mg#.

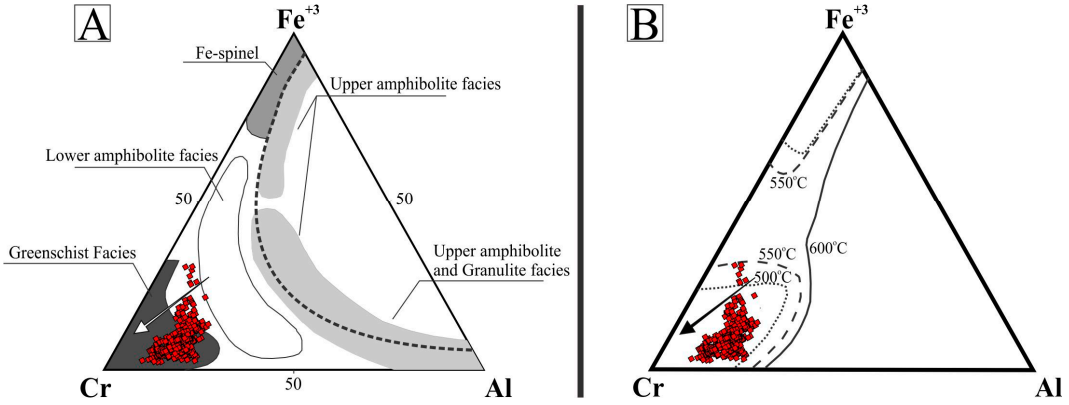

Figure 6. Ternary Cr–Al–Fe^{3+} diagrams exhibiting >500 analyses of chromite from Cedrolina. (**A**) Modified after [11], with the fields of different metamorphic facies from [39–41]; (**B**) Stability limits of spinels defined for chromite and magnetite (calculated in equilibrium with Fo90 olivine). Modified after [42,43]. Both arrows (black and white) indicate the direction of metamorphic retrogression to greenschist facies.

4.2. Rutile

Rutile is an abundant accessory mineral in the investigated chromitite and is found in almost all samples, representing up to ~2% of modal composition. It occurs as small needles/prisms (less than 5 μm) included in chromite (Figure 7A), as larger prisms in the matrix mostly defining the main metamorphic foliation and as anhedral grains (>100 μm) in the chromite/matrix interface (Figure 7B–D). Some anhedral crystals (sometimes over 200 μm) are found filling fractures inside chromium spinel (Figure 7E). Porphyroblastic anhedral grains of rutile occasionally contain micro-inclusions of chromite fragments (Figure 7B,D,F).

All analyzed rutiles have constantly high concentrations of Cr (from 12,800 to 39,200 ppm, samples 100 and 105, respectively), W (up to 6840 ppm, sample 105), Nb (up to 4090 ppm, sample 100), and V (all above 4000 ppm) (Table 3). Rutile is known to be the dominant carrier of high field-strength elements (HFSE) (up to 90% of whole rock content of Ti, Nb, Ta, W, and Sb) and an important carrier (up to 45% of whole rock content) of Cr and Nb [15]. Therefore, high concentrations of Nb, Cr, W, and V in the analyzed rutiles reflect high availability of these elements in the studied system. Although maximum concentrations can be very high, trace element data show a large spread, either between different samples or within a single one (Table 3).

As previously mentioned, Zr content in rutile is temperature dependent [16,44]. The analyzed rutiles show Zr contents ranging from less than 55 ppm (EPMA minimum detection limit) to 540 ppm. With one exception (410 ppm for one analysis in sample 105), values above 200 ppm of Zr are only obtained in sample 100. Analyzed samples can be divided into two different groups according to their trace element contents. Samples 47 and 105 have the highest Cr and W contents and the lowest concentrations of Nb and Zr. Samples 14, 100, 106 have the lowest Cr and W contents. However, within this group, samples 14 and 106 have low Nb and Zr content. Rutiles from sample 100 have the highest Zr and Nb content of all samples (up to 540 ppm). It is important to mention that there is no systematic variation on trace element contents between rutiles included in chromites and in the matrix. As an attempt to estimate temperature of rutile crystallization, the Zr-in-rutile geothermometer (calibration of [44]) was applied. The results are shown in Figure 2, where dashed blue lines represent the temperatures calculated for analyses contained in Table 3. Although pressure has an influence on the calculated temperature, its effect is below 35 °C for the calculated range (0.2 to 1.0 GPa). Within this pressure range, calculated temperatures vary from circa 500 to 650 °C. It has to be stressed that calculated temperatures represent maximum temperatures, as the studied rocks are quartz free (silicates as chlorite and talc are present, though). Furthermore, zircon and baddeleyite coexist and indicate that silica activity ($aSiO_2$) is low. However, maximum uncertainties

introduced to rutile thermometry by unconstrained $aSiO_2$ are 60 to 70 °C at 750 °C [45]. Since the country rocks (amphibolites and amphibole schists of the Cedrolina Formation) have a metamorphic assemblage composed of hornblende, andesine, magnetite, and garnet (chlorite and clinopyroxene free), the reactions "Chl-out" and E + Qtz = An + Grt + Mt + F (Figure 2) provide a reasonable 0.4 to 0.6 GPa pressure estimate. Temperatures calculated for a pressure of 0.4 GPa are presented in Table 3. For samples 14, 105, and 106 (samples from the main chromitite body), the Zr data results in an average temperature of 550 °C (510 to 650 °C). An average temperature of 600 °C (510 to 670 °C) is calculated for sample 100. Although temperatures may be slightly high due to the unconstrained $aSiO_2$, within the error, average temperatures calculated for samples from the main chromitite body are in accordance with metamorphic conditions reported for the area.

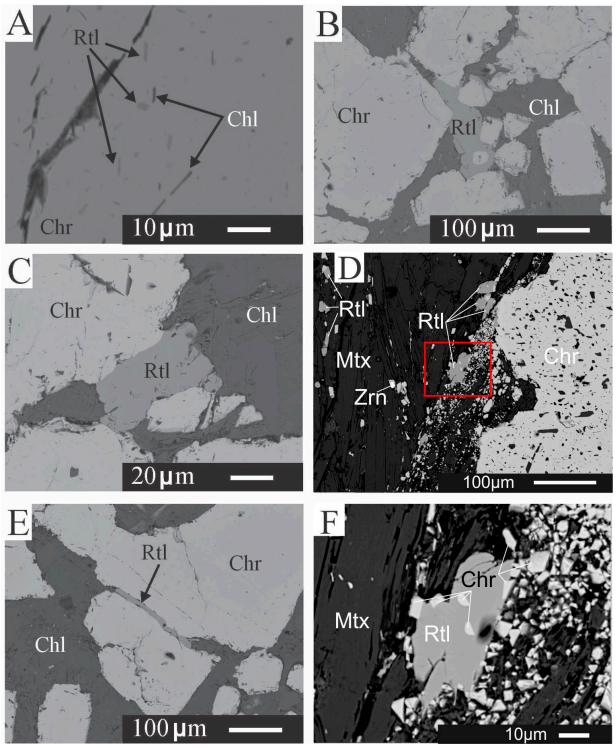

Figure 7. BSE images of different forms of occurrence of rutile in the Cedrolina chromitite (**A**) Plenty of prismatic micro inclusions (<10 µm) of rutile and chlorite in chromite; (**B**) Large anhedral/irregular rutile crystal in the chromite/chlorite contact, also exhibiting an included chromite fragment; (**C**) Anhedral rutile crystal observed in the chromite/matrix interface; (**D**) Rutile porphyroblasts/prisms concordantly oriented with the metamorphic foliation (Fn is vertical in the photo) and often presenting inclusions of chromite fragments, situated near the edge of a large Cr-spinel aggregate. Area of red rectangle zoomed in (F); (**E**) Elongated and anomalously large rutile crystal (>250 µm) that fills a fracture between two large chromite fragments; (**F**) Zoomed area of red rectangle in (D) displaying a rutile porphyroblast with abundant micro-inclusions of chromite fragments. Abbreviations: Chr = chromite; Chl = chlorite; Mtx = matrix; Rtl = rutile; Zrn = zircon.

Table 3. Selection of representative electron microprobe trace element analyses of rutile from Cedrolina chromitite (ppm).

Sample CED	Mg	Nb	Cr	Al	W	Fe	Zr	V	T °C
D.L.	30	110	45	30	135	30	55	30	-
47	80	150	23,100	230	550	560	bd	4530	-
47	110	bd	25,100	210	3900	580	bd	4570	-
47	50	bd	24,200	210	390	1040	bd	4520	-
106	bd	680	18,200	150	1180	850	bd	4320	-

Table 3. *Cont.*

Sample CED	Mg	Nb	Cr	Al	W	Fe	Zr	V	T °C
106	bd	300	17,200	140	1410	790	170	4430	580
14	210	bd	8110	140	350	1440	bd	5060	-
14	70	bd	8940	210	bd	1370	60	4770	510
14	160	bd	7480	140	bd	1660	bd	5220	-
14	bd	140	9650	130	230	1490	bd	4910	-
105	bd	230	24,000	200	4180	580	90	4700	540
105	80	350	26,100	260	3120	540	bd	5000	-
105	100	490	26,300	250	3640	1030	70	4590	530
105	60	320	21,600	220	3360	430	bd	4730	-
105	bd	150	26,100	180	4340	770	60	4570	510
105	1330	170	24,300	240	5550	800	410	4700	650
105	70	360	23,700	210	6560	510	bd	5370	-
105	90	390	39,200	220	5090	1130	90	4700	540
105	40	380	25,400	180	6840	620	80	4850	530
105	50	420	33,500	220	6570	1480	bd	4470	-
100	40	650	14,300	150	870	860	430	5160	650
100	bd	1220	14,700	140	1080	1160	70	4740	520
100	40	900	14,100	200	470	1280	260	5240	610
100	30	4090	15,400	130	1140	640	bd	5080	-
100	bd	440	15,100	170	2970	780	540	4710	670
100	bd	560	12,800	180	630	750	60	4730	510

Mn concentrations are always below the detection limit (bd) of 100 ppm. Temperatures were calculated for a pressure of 0.4 GPa using the calibration of [44]. D.L.: detection limit.

4.3. Zircon

Zircon is a minor but common phase in the studied chromitite. It forms grains variable in size from 5–100 µm (Figure 8), generally exhibiting euhedral shapes. Zircon mainly occurs in the silicate matrix (Figure 7D), locally in contact with chromite (Figure 8A) and rutile (Figure 8D) and rarely as inclusions in chromite. The crystals may display apparently zoned morphologies (Figure 8A,B) which, nonetheless, do not correspond to chemical variations in Si, Zr, Hf, Th, and U (Figure 9), attesting a homogeneous distribution of these elements.

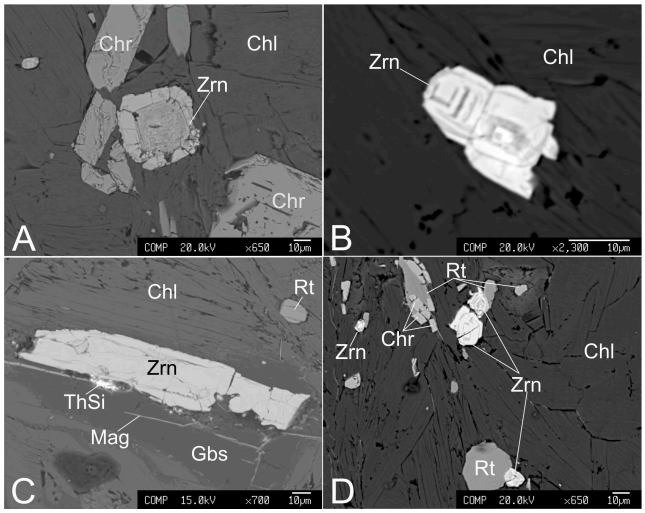

Figure 8. BSE images of zircon crystals in the matrix (sample 105C). (**A**) and (**B**) Apparently zoned crystals; (**C**) Mega-crystal associated with a Th-silicate. The dark gray mass around zircon is gibbsite with thin bands of magnetite (light gray); (**D**) Zircon crystals in close association with rutile in the matrix. Abbreviations: Chl = chlorite, Chr = chromite, Gbs = gibbsite, Mag = magnetite, Rt = rutile, ThSi = Th-silicate, Zrn = zircon.

Table 4. Selection of representative electron microprobe analyses of zircon from Cedrolina chromitite (wt %).

Sample CED	SiO_2	ZrO_2	Al_2O_3	FeO	Cr_2O_3	TiO_2	HfO_2	Y_2O_3	Nb_2O_5	UO_2	ThO_2	Ce_2O_3	La_2O_3	Nd_2O_3	Pr_2O_3	Total
105C	34.09	63.36	0.3	0.54	0.81	0.07	0.9	0.33	0	0.07	0	0.08	0	0.27	0	100.81
105C	33.62	62.26	0.5	0.63	0.31	0.11	1.29	0.24	0.04	0.11	0.11	0.09	0.03	0.79	0.06	100.19
105C	33.69	62.84	0.63	0.75	0.41	0.11	0.92	0.38	0.06	0.11	0.13	0.18	0.07	1.18	0.02	101.47
105C	33.82	63.45	0.22	0.45	0.59	0.07	0.83	0.64	0.04	0.14	0.03	0.08	0.07	0.14	0	100.57
105C	34.01	63.51	0.18	0.37	0.62	0.1	0.89	0.35	0.05	0.09	0.02	0.03	0	0	0.08	100.3
105C	32.42	62.41	0.95	0.7	0.43	0.15	1.17	0.26	0.02	0.18	0.19	0.07	0	0.88	0	99.84
105C	32.11	63.4	0.54	0.56	0.51	0.1	1.23	0.16	0.02	0.12	0.08	0	0	0	0	98.83

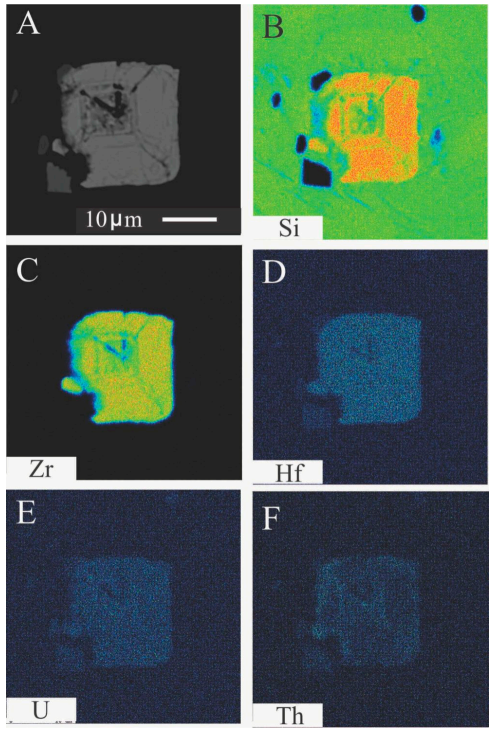

Figure 9. (**A**) Zircon BSE image; (**B**–**F**) Elemental distribution map.

Microprobe analyses (Table 4) also indicate high ∑REE contents (av. ~1.0 wt %) and TiO_2 ranging from 0.07–0.15 wt % (420–900 ppm of Ti). Temperatures calculated by the Ti-in-zircon thermometer are much higher (~1200–1400 °C) than the local metamorphic temperature. This is due to the very low $aSiO_2$ (~0.1) in the rocks, reflected by the absence of quartz, which is known to enhance uptake of Ti in zircon [46]. Concentrations of selected trace elements, such as Hf, Y, and U, are compared with the compositional fields of zircon associated with different rock types (Figure 10), as proposed by [19]. According to these diagrams, the zircons in the Cedrolina chromitite have a geochemical signature that differs from those of kimberlitic and carbonatitic sources, but are very similar to zircons reported from syenites, granitoids, and larvikites.

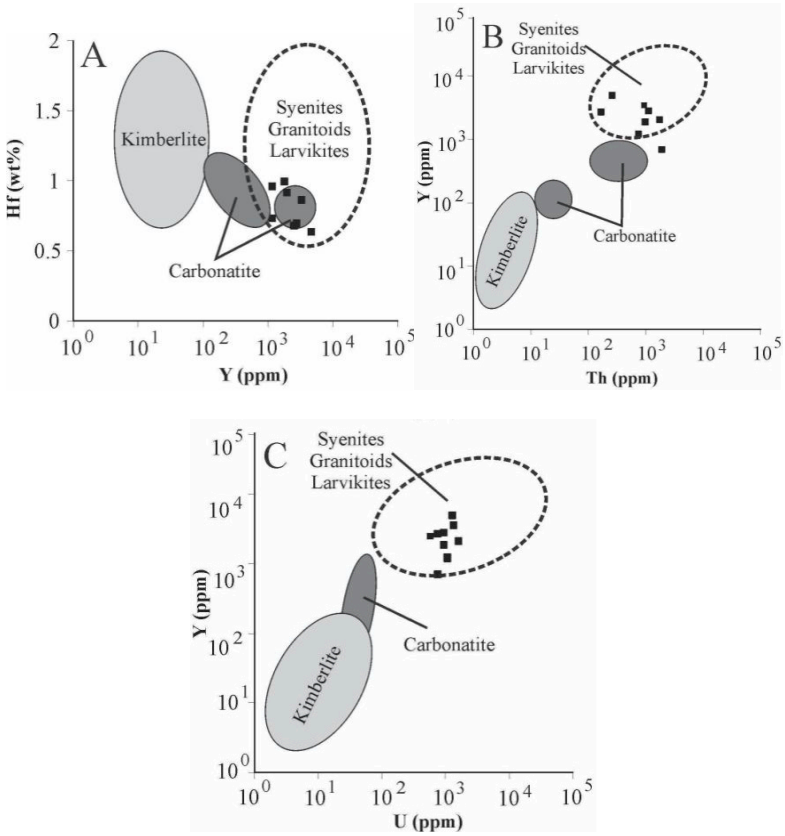

Figure 10. Trace element plots from accessory zircons found in the Cedrolina chromitite. Different source rock fields adapted from [19]. (**A**) Hf vs. Y; (**B**) Y vs. Th; (**C**) Y vs. U.

4.4. PGM, Au and Ag Phases

PGM, Au and Ag phases are very rare in the studied chromitite. They form very small grains, less than 10 μm in size (Figure 11). Thus, the composition of most of these phases was only qualitatively determined by EDS analyses. The following PGM were identified: laurite [RuS_2] (Figure 11F) and irarsite [(Ir,Ru,Rh,Pt)AsS] (Figure 11B,F) (too small to be quantitatively analyzed). They occur included in chromite (Figure 11B) or in contact with chlorite from the matrix (Figure 11F). Only one grain composed of Au and Pd was large enough to be quantitatively analyzed, and its stoichiometry was calculated as Au_3Pd (Table 5). The Au_3Pd was found at the chromite/matrix interface (Figure 11C). Small grains of pure gold (Figure 11A) and one alloy composed of Au, Cu, and Ni (Figure 11D) were also recognized. They occur at the contact between chromite and talc or in the silicate matrix. According to the quantitative analyses, the alloy has the following stoichiometry: Au_3Cu_3Ni (Table 5). Silver-bearing minerals occur included (Figure 11E) or in contact with chromite. Based on qualitative analyses they have been tentatively classified as pearceite (Figure 11E) and argentite.

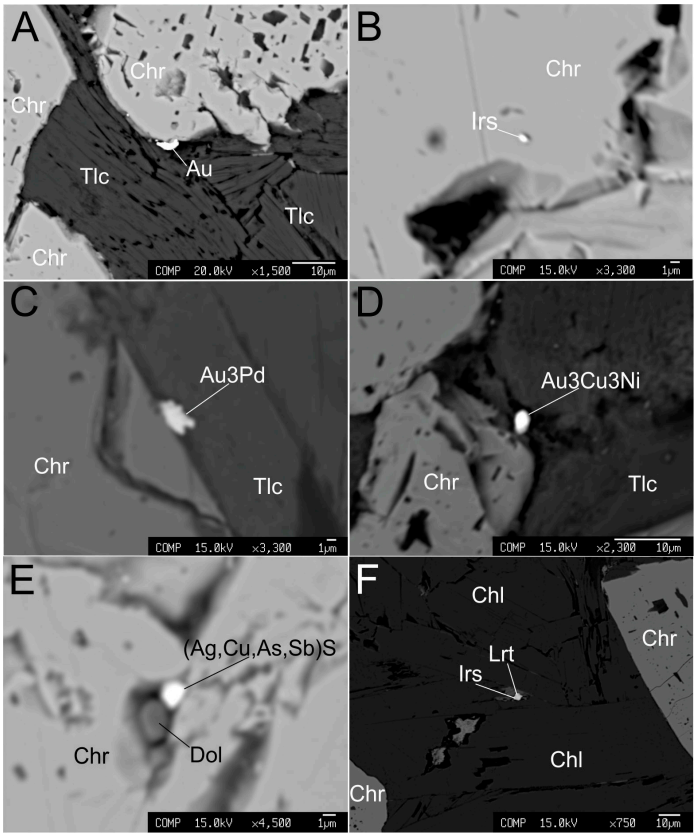

Figure 11. BSE images of PGM, Au and Ag minerals. (**A**) Native gold at the chromite/matrix interface; (**B**) Irarsite included in chromite; (**C**) Unnamed gold and palladium alloy (Au_3Pd) in the chromite/matrix interface; (**D**) Unnamed gold, copper and nickel alloy (Au_3Cu_3Ni) in the chromite/matrix interface; (**E**) Unidentified silver, copper, arsenic and antimony sulfide (possibly pearceite: $[(Ag_8CuS_4)][(AgCu)_6(As,Sb)_2S_7]$) included in chromite; (**F**) Laurite and irarsite association in the matrix. Abbreviations: (Ag,Cu,As,Sb)S = unidentified sulfide, Au = gold, Au_3Pd = unnamed PGE alloy, Au_3Cu_3Ni = unnamed gold alloy, Chr = chromite, Chl = chlorite, Dol = dolomite, Irs = irarsite, Lrt = laurite, Tlc= talc.

Table 5. Electron microprobe analyses of Au and Pd minerals from the Cedrolina chromitite.

	Au_3Pd			Au_3Cu_3Ni							
Sample	**105C**	**106D**	**106D**	**47A**	**47A**	**47A**	**47A**	**47A**	**47A**	**47A**	**47A**
						wt %					
Pd	14.15	14.55	13.81	0	0	0	0	0	0	0	0
Au	80.18	81.57	79.27	65.44	67.33	68.34	68.29	69.14	65.92	69.94	63.38
Cu	n.a.	n.a.	n.a.	22.5	21.75	24.75	22.8	22.67	25.41	23.36	24.16
Ni	n.a.	n.a.	n.a.	6.78	6.59	7.29	6.69	6.64	7.78	6.85	7.36
Total	94.33	96.12	93.09	94.71	95.68	100.38	97.78	98.44	99.12	100.14	94.9
						at %					
Pd	24.59	24.81	24.37	0	0	0	0	0	0	0	0
Au	75.41	75.19	75.63	41.48	42.95	40.35	42.35	42.8	38.63	42.34	38.92
Cu	n.a.	n.a.	n.a.	44.13	42.95	45.24	43.75	43.43	46.09	43.77	45.92
Ni	n.a.	n.a.	n.a.	14.4	14.1	14.42	13.9	13.77	15.28	13.89	15.16
						apfu					
Pd	0.98	0.99	0.97	0	0	0	0	0	0	0	0
Au	3.02	3.01	3.03	2.9	3.01	2.82	2.96	3	2.7	2.96	2.72
Cu	n.a.	n.a.	n.a.	3.09	3.01	3.17	3.06	3.04	3.23	3.06	3.21
Ni	n.a.	n.a.	n.a.	1.01	0.99	1.01	0.97	0.96	1.07	0.97	1.06

n.a. = not analyzed; apfu = atoms per formula unit; at % results are normalized to 100%; low wt % totals are due to analytical errors associated with the small size of the grains.

4.5. Other Accessory Minerals

A great number of other accessory phases have been found in the Cedrolina chromitite. All of them have been only qualitatively analyzed, owing to their small size (in most cases, less than 5 μm). They are very rare and, with few exceptions, occur in the weathered silicate matrix. In particular, the following minerals have been identified: uraninite, thorianite, baddeleyite, ilmenite, magnetite, apatite, dolomite, barite, heazlewoodite, chalcopyrite, sphalerite, arsenopyrite, and a compound composed of Hg and Se (possibly tiemanite). Uraninite was found included in chromite as a single phase or associated with rutile. Confirming the previous finding of [14], several grains of monazite-Ce have been also recognized mostly in the silicate matrix.

5. Discussion

5.1. Origin of the Cedrolina Chromitite

Field relationships indicate that the Cedrolina chromitite is hosted by talc-chlorite schist. The ore body is small (230 × 100 m), tabular and exhibits a metamorphic foliation (Fn) which is concordant with that found in the country rocks. The structure of the chromitite is quite distinct, and is characterized by large (0.5–1.5 cm) spherical to ellipsoidal nodules of chromite immersed in a silicate matrix (talc + chlorite). This structure is very similar to those reported in the chromitite hosted ophiolitic chromitite. Nodular structure is typical of chromitites that crystallized from a boninitic magma enriched in water in a suprasubduction zone environment, as evidenced by experimental observation [47].

However, the composition of Cedrolina chromite does not properly fit into any of the fields proposed to discriminate stratiform and podiform chromitites (Figure 5B). The absence of alteration rims or compositional zoning, coupled with macroscopic and microscopic observations of the chromite and matrix, indicates the complete obliteration of the primary magmatic composition by metamorphic processes. This statement is also supported by the fact that chromite shows high Cr# (0.80–0.86) and high Fe^{2+}# (0.70–0.94) consistent with variation trends of spinels from metamorphic rocks. Ternary diagrams presented in Figure 6 show that the Cedrolina chromite has a composition equivalent to spinel metamorphosed in the greenschist facies (500–550 °C), which overprinted its original (higher) magmatic crystallization temperature. Metamorphism is also attested by the presence of Cr-rich chlorite (kammererite) in the matrix and magnetite ex-solutions near/in chromite, indicating that Cr and Fe^{2+} were remobilized from chromite, which had originally higher contents of these elements.

Likewise, high Cr_2O_3 content in rutile is interpreted to be related to Cr remobilization from chromite during metamorphism. Anhedral and porphyroblastic (>100 μm) grains that fill fractures in chromite give a strong evidence that rutile crystallized after the Cr-spinel nodules had been fractured/brecciated, which also justifies common micro-inclusions of chromite fragments in rutile due to metamorphic overgrowth. Furthermore, prismatic rutile crystals (with or without chromite inclusions) and trails of chromite fragments, along with platy chlorite define a strong metamorphic foliation (Fn), indicating that the deformation of the nodules and rutile genesis are both linked to the same metamorphic event, with deformation prior to or synchronous with metamorphism. In addition, this chronology connotes that the chromite nodules must have been solid or at least rigid enough to be fractured at the time of deformation, otherwise they would have only suffered plastic/ductile deformation and, hence, display predominantly coalescent contacts between orbs (alike the leopard chromite from Troodos ophiolite, Cyprus), which is not the case. Moreover, this causal sequence argues that the observed nodules must have been formed before metamorphic peak, although recrystallization during it could have also played a role in erasing/amalgamating formerly sharp contacts within orbs (generating massive nodules) or creating polygonal contacts within previously massive nodules.

The crystallization temperature of rutile and, by inference, the metamorphic peak of the area is estimated at 550–600 °C (at an estimated pressure of 0.4–0.6 GPa), which is in agreement with the superior metamorphic temperature range defined by chromite composition (~550 °C, Figure 6B),

metamorphic paragenesis of amphibolites from the Cedrolina area (>570 °C) and the low amphibolite facies conditions described in literature. Assuming that Ti available to crystalize rutile was remobilized from chromite, the abundance of rutile (av. ~0.5% of the modal composition) dispersed in the matrix would also be an indicative that chromite was originally Ti-rich, which is typical for stratiform chromitites and could explain the few analyses that plot in their field (Figure 5A). In order to evaluate this hypothesis, mass balance calculations were performed as an attempt to reintegrate all the Ti content of the whole rock into chromite. Calculations were carried out assuming 60% and 0.5% average modal abundance of chromite and rutile, respectively, and that rutile is composed by 96 wt % of TiO_2 (in av.). Rutile was assumed to be, besides chromite, the only Ti bearing phase. With these parameters, maximum TiO_2 contents of about 1 wt % (from 0.80 to 2.16 for the chromite analyses presented in Table 2) can be calculated for the chromites. If the modal abundance of rutile is doubled (i.e., 1%), calculated concentrations of Ti in chromite increase about 50% to 70% (1.60 to 2.96), since the concentration already present in chromite has to be taken into account (as high as 1.36, Table 2).

It is as well critical to assess the possibility that titanium could have been introduced by external sources, thus not belonging to the parental magma composition. In that sense, it has been documented that aqueous solutions with substantial amounts of hydrocarbons could effectively leach Ti from igneous rocks and re-precipitate titanium bearing minerals in sedimentary [48] and subduction zone [49] environments. The transport of Ti and other elements (Sn, REE, U, and Zr) is also believed to be favoured by fluoride, which increases rutile solubility in high-temperature hydrothermal fluids due to the formation of mixed hydroxofluoro-complexes [50] (and references therein). It has also been shown that both zircon and rutile can crystallize from alkali and Al–Si bearing aqueous fluids [51] in quartz veins emplaced in HP/UHP terrains (in [52]). However, no carbon-enriched rocks are found in about 2 km radius far from the Cedrolina chromitite, greatly diminishing the possibility that Ti could have been re-mobilized by hydrocarbon solutions from external sources.

In spite of that, the possibility that chromite was titanium rich is extremely controversial, considering that it is currently widely accepted that Ti-rich chromites are typical of stratiform deposits, and not of ophiolite complexes. Also the observation of a microscopic texture in which nodules of chromite are formed by aggregates of fine euhedral chromite crystals that exhibit sharp/straight contacts with each other (resembling a cumulus texture, Figure 4C,D) as well as the presence of what indeed appears to be cumulus texture (Figure 4F) are both common characteristics of stratiform chromitites. High MnO (>0.14 wt %) contents are, as well, typical of stratiform chromitites [53]. Compiling all the information it is possible to withdraw two alternatives to explain the origin of the studied chromitite:

1. The Cedrolina chromitite is podiform, and therefore associated with a Precambrian ophiolite. In this case, it would imply that either the parental magma of the chromitite (rich in Ti) was chemically different from all other magmas associated with ophiolitic complexes known to date (low Ti) or that titanium was added by external sources/fluids and the internal polygonal texture of nodules is solely due to metamorphic recrystallization.
2. The Cedrolina chromitite is stratiform, hence associated with mafic–ultramafic (high Ti) intrusions. If this alternative is valid, the structure observed in chromite could be understood as a new type of metamorphic orbicular structure that has not been described in the literature. The chromite nodules may have been formed by aggregates of fine euhedral chromite crystals resembling a cumulus texture as shown in Figure 4B–D. The straight contacts, as well as the triple junctions as shown in Figure 4D, may represent an original cumulus texture which was not completely obliterated by recrystallization. This observation could constitute another argument in favour of a cumulitic-stratiform origin.

Both models are plausible and imply post-magmatic and recrystallization processes. Notwithstanding, it is still unclear how much of the recrystallization process is influenced by metamorphism as a result of the poly-metamorphic history of the area. It is important to state that the authors comprehend that these models are merely theoretical.

5.2. The Accessory Minerals in the Cedrolina Chromitite and Their Petrogenetic Significance

The most common and studied accessory minerals that occur in chromitites are PGM, base metals sulphides and arsenides. On the basis of their textural relationships, occurrence and composition, the PGM have been divided into (1) primary, formed in the magmatic stage, before and during the precipitation of chromite and (2) secondary, formed by the alteration of primary PGM at a relatively low temperature [2–12]. Paragenetic considerations indicate that in the Cedrolina chromitite only irarsite and laurite could represent relicts of the original igneous assemblage [54–59]. On the contrary, the Pd–Au together with Au–Cu–Ni alloys and gold, are more likely formed during post magmatic processes, as suggested by Pd mobility at low temperatures described in the Bacuri complex of Brazil [60]. Regarding rutile composition, different trace element contents from samples 14, 47, 105, and 106 may be due to variations on the whole rock chemistry within the main chromitite body or reflect heterogeneous enrichment/incorporation of trace elements by metasomatism/hydrothermal fluids. Sample 100 was collected about 300 m to the South, close to a felsic intrusion. High Zr and Nb content in sample 100 may be due to intense hydrothermal metasomatism associated with fluids emanating from this albite-granite intrusion. The high chromium content of rutile (up to 39,200 ppm) is interpreted to be due to Cr remobilization from chromite. The exotic accessory minerals found in the Cedrolina chromitite, such as monazite-Ce, uraninite, thorianite, zircon, and Ag-phases are believed to have precipitated from an external fluid. The necessary incompatible elements to form these uncommon accessory minerals were probably supplied by hydrothermal solutions emanating from a neighboring albite-granite gneiss, which is correlative with the felsic intrusions of the Pilar de Goiás Greenstone Belt described by [24]. This assumption is also supported by the composition of the accessory zircon analyzed in the Cedrolina chromitite, whose trace element signature/distribution points to a granitoid origin/affinity (Figure 10). The high ∑REE contents in zircon (av. ~1 wt %) and TiO_2 ranging from 0.07–0.15 wt % (420–900 ppm of Ti) are also suggestive of a granitic source rock as proposed by [19]. This hydrothermal activity coupled with intense lateritic weathering were seemingly responsible for the genesis of a wide range of supergene accessory minerals, such as Al/Mg hydroxides (after chlorite), carbonates, and phosphates (commonly hydrated) containing various amounts of Ca, Mg, Ba, and rarely Ni, Fe, and REE (probably after monazite weathering), as well as abundant barite. The relative age of the chromitites could be estimated by certain temporal relationships between the country rocks and regional deformational phases. The supposed enrichment in incompatible elements, if indeed related to hydrothermal fluids that emanated from felsic intrusions, implies that the chromitites are older than such intrusions. Considering this assumption true, the concordant U–Pb ages of 2145 ± 12 Ma obtained by [24] in albite granites that intrude the Pilar de Goiás Greenstone Belt, could be used to stipulate that the chromitites are older than 2.1 Ga and, therefore, Paleoproterozoic or Archean.

6. Conclusions

1. The Cedrolina chromitite exemplifies a completely metamorphosed chromitite.
2. The main regional metamorphic peak reached the low amphibolite facies, with temperatures of 550–600 °C at an estimated pressure range of 0.4–0.6 GPa. This event was responsible for the complete obliteration of chromite magmatic composition.
3. Among the studied accessory minerals, only irarsite and laurite could be relicts of the primary igneous assemblage, whereas Au–Pd and Au–Cu–Ni compounds are likely products of low-temperature remobilization and recrystallization of the igneous phase, arguably under weathering/supergene conditions.
4. The precipitation of exotic accessory minerals found in the Cedrolina chromitite is probably related with metasomatism promoted by hydrothermal fluids derived from a granitic intrusion that occurs in the same area. Although not confirmed, this theory is supported by accessory zircon (found in the chromitite) trace element composition, which suggests a granitoid source.

5. Rutile likely formed due to Ti remobilization from Cr-spinel after/synchronously to chromite deformation/fracturing during the main metamorphic and deformational event (Dn). Geothermometric calculations resulted in a crystallization temperature range of 510–670 °C (averaging 550–600 °C at an estimated pressure range of 0.4–0.6 GPa) concordant with an upper greenschist to low amphibolite facies metamorphic grade. Thus, it suggests that the magmatic composition of chromite could have been originally higher in Ti, indicating a stratiform origin. Alternatively, the Ti-enrichment could have been caused by external metasomatic infiltrating fluids leading to the formation of rutile. If this was the case, the Cedrolina chromitites could be classified as podiform, possibly representing a sliver of tectonically dismembered Paleoproterozoic upper mantle.
6. The nodular structure observed in the Cedrolina chromitite resembles those described in ophiolitic chromitites. However, it could also be interpreted as a new type of metamorphic structure which was not previously described in literature. The orbs feasibly formed by post-magmatic and partial recrystallization processes, however, it is still unclear to what extent metamorphism controlled recrystallization due to the poly-metamorphic history of the area.
7. The Cedrolina chromite composition in terms of Cr# and Mg# plots outside the fields of both podiform and stratiform chromitites, being characterized by high values of Cr# and low Mg#. They display a very restricted and highly refractory composition of Cr-spinel (high Cr#). Therefore, it differs from the Neoproterozoic ophiolitic chromitite of the Eastern Desert of Egypt and Saudi Arabia [35–38] that can be classified as Cr- and Al-rich. Regarding their TiO_2 content, few analyses of the Cedrolina chromitite plot in the field of stratiform chromitite (occurring in layered complexes).
8. The strong metamorphic overprint that affected the studied chromitites has made it dubious to define their original geodynamic setting and to properly classify them as podiform or stratiform.

Acknowledgments: We thank the University Centrum for Applied Geosciences (UCAG) for providing access to the Eugen F. Stumpfl electron microprobe Laboratory (University of Leoben, Austria). Three anonymous reviewers provided constructive and helpful corrections and comments. Many thanks are also in order to the editorial staff of Minerals. Alan E. Boudreau is thanked for his useful comments on an early version of the manuscript.

Author Contributions: Yuri de Melo Portella wrote the manuscript, conducted the fieldwork and sample collection. Federica Zaccarini along with Yuri de Melo Portella collected the microprobe data. George L. Luvizotto elaborated the data of rutile and Ronald J. Bakker analyzed the rutile by Raman. All the authors, including Giorgio Garuti, Nelson Angeli and Oskar Thalhammer were involved during the interpretation of the data and provided valuable ideas for the discussion.

Conflicts of Interest: The authors declare no conflict of interest.

References

1. Tropper, P. Small grains and big implications: Accessory Ti- and Zr-minerals as petrogenetic indicators in HP and UHP marbles. *Am. Mineral.* **2014**, *99*, 1197–1198. [CrossRef]
2. Stockman, H.W.; Hlava, P.F. Platinum-group minerals in Alpine chromitites from southwestern Oregon. *Econ. Geol.* **1984**, *79*, 491–508. [CrossRef]
3. Bowles, J.F.W. The development of platinum-group minerals in laterite. *Econ. Geol.* **1986**, *81*, 1278–1285. [CrossRef]
4. Garuti, G.; Zaccarini, F. In-situ alteration of platinum-group minerals at low temperature: Evidence from chromitites of the Vourinos complex, Greece. *Can. Mineral.* **1997**, *35*, 611–626.
5. Garuti, G.; Proenza, J.A.; Zaccarini, F. Distribution and mineralogy of platinum-group elements in altered chromitites of the Campo Formoso layered intrusion (Bahia State, Brazil): Control by magmatic and hydrothermal processes. *Mineral. Petrol.* **2007**, *89*, 159–188. [CrossRef]
6. Garuti, G.; Zaccarini, F.; Proenza, J.A.; Thalhammer, O.A.R.; Angeli, N. Platinum-group minerals in chromitites of the Niquelândia layered intrusion (Central Goias, Brazil): Their magmatic origin and low-temperature reworking under serpentinization and lateritic weathering. *Minerals* **2012**, *2*, 365–384. [CrossRef]

7. Zaccarini, F.; Proenza, J.A.; Ortega-Gutierrez, F.; Garuti, G. Platinum group minerals in ophiolitic chromitites from Tehuitzingo (Acatlan complex, southern Mexico): Implications for postmagmatic modification. *Mineral. Petrol.* **2005**, *84*, 147–168. [CrossRef]
8. Zaccarini, F.; Pushkarev, E.; Garuti, G. Platinum-group element mineralogy and geochemistry of chromitite of the Kluchevskoy ophiolite complex, central Urals (Russia). *Ore Geol. Rev.* **2008**, *33*, 20–30. [CrossRef]
9. Zaccarini, F.; Proenza, J.A.; Rudashevsky, N.S.; Cabri, L.J.; Garuti, G.; Rudashevsky, V.N.; Melgarejo, J.C.; Lewis, J.F.; Longo, F.; Bakker, R.J.; et al. The Loma Peguera ophiolitic chromitite (Central Dominican Republic): A source of new platinum group minerals (PGM) species. *J. Mineral. Geochem.* **2009**, *185*, 335–349. [CrossRef]
10. Proenza, J.A.; Zaccarini, F.; Lewis, J.F.; Longo, F.; Garuti, G. Chromian spinel composition and the platinum-group minerals of the PGE-rich Loma Peguera chromitites, Loma Caribe peridotite, Dominican Republic. *Can. Mineral.* **2007**, *45*, 211–228. [CrossRef]
11. Proenza, J.A.; Zaccarini, F.; Escayola, M.; Cábana, C.; Schalamuk, A.; Garuti, G. Composition and textures of chromite and platinum-group minerals in chromitites of the western ophiolitic belt from Pampeans Ranges of Córdoba, Argentina. *Ore Geol. Rev.* **2008**, *33*, 32–48. [CrossRef]
12. Aiglsperger, T.; Proenza, J.A.; Zaccarini, F.; Lewis, J.F.; Garuti, G.; Labrador, M.; Longo, F. Platinum group minerals (PGM) in the Falcondo Ni-laterite deposit, Loma Caribe peridotite (Dominican Republic). *Mineral. Depos.* **2015**, *50*, 105–123. [CrossRef]
13. Zaccarini, F.; Garuti, G.; Martin, R. Exotic accessory minerals in layered chromitites of the Campo Formoso complex (Brazil). *Geol. Acta* **2006**, *4*, 461–469.
14. Zaccarini, F.; Portella, Y.M.; Bakker, R.J.; Angeli, N.; Garuti, G.; Thalhammer, O.A.R. Electron microprobe and Raman spectroscopic investigation of monazite from chromitites of Cedrolina, (Goias State, Brazil). *J. Mineral. Geochem.* **2012**, *189*, 207–215. [CrossRef] [PubMed]
15. Zack, T.; Kronz, A.; Foley, S.F.; Rivers, T. Trace element abundances in rutile from eclogites and associated garnet mica schists. *Chem. Geol.* **2002**, *184*, 97–122. [CrossRef]
16. Zack, T.; Moraes, R.; Kronz, A. Temperature dependence of Zr in rutile: Empirical calibration of a rutile thermometer. *Contrib. Mineral. Petrol.* **2004**, *148*, 471–488. [CrossRef]
17. Luvizotto, G.L.; Zack, T. Nb and Zr behavior in rutile during high-grade metamorphism and retrogression: An example from the Ivrea-Verbano Zone. *Chem. Geol.* **2009**, *261*, 303–317. [CrossRef]
18. Luvizotto, G.L.; Zack, T.; Triebold, S.; von Eynatten, H. Rutile occurrence and trace element behavior in medium-grade metasedimentary rocks: Example from the Erzgebirge, Germany. *Mineral. Petrol.* **2009**, *97*, 233–249. [CrossRef]
19. Belousova, E.; Griffin, W.; O'Reilly, S.Y.; Fisher, N. Igneous zircon: Trace element composition as an indicator of source rock type. *Contrib. Mineral. Petrol.* **2002**, *143*, 602–622. [CrossRef]
20. Portella, Y.M. Mapeamento Geológico, Caracterização Litoquímica e Potencial Econômico do Corpo de Cromitito de Cedrolina, Santa Terezinha de Goiás-GO. Unpublished Bachelor's Thesis, São Paulo State University (UNESP), Rio Claro, Brazil, 2011. (In Portuguese)
21. Jost, H.; Fuck, R.; Brod, J.A.; Dantas, E.L.; Meneses, P.R.; Assad, M.L.; Pimentel, M.M.; Blum, M.L.B.; Silva, A.; Spigolon, A.L.D. Geologia de terrenos Arqueanos e Proterozóicos da região de Crixás-Cedrolina, Goiás. *Rev. Bras. Geociên.* **2001**, *31*, 315–328. (In Portuguese)
22. Ribeiro Filho, W. Reavaliação da geologia de Pilar-Mara Rosa. *Simp. Geol.* **1981**, *1*, 281–296. (In Portuguese)
23. Lacerda, H. Mapa geológico 1/100.000 do distrito mineiro do Greenstone-Belt de Crixás-Guarinos-Pilar de Goiás (GO). In Proceedings of the Anais do IV Simpósio de Geologia do Centro-Oeste, Cuiabá-MT, Brazil, 26–31 Outubro de 1997; Departamento Nacional de Produção Mineral: Goiânia, Brazil, 1997. (In Portuguese)
24. Queiroz, C.L. Evolução Tectono-Estrutural dos Terrenos Granito-Greenstone Belt de Crixás, Brasil Central. Unpublished Ph.D. Thesis, University of Brasília, Brasília, Brazil, 2000. (In Portuguese)
25. Jost, H.; Chemale, F., Jr.; Dussin, I.A.; Tassinari, C.C.G.; Martins, R. A U–Pb zircon Paleoproterozoic age for the metasedimentary host rocks and gold mineralization of the Crixás greenstone belt, Goiás, Central Brazil. *Ore Geol. Rev.* **2010**, *37*, 127–139. [CrossRef]
26. Jost, H.; Scandolara, J.E. Características estruturais, petrográficas e geoquímicas de enxame de diques máficos intrusivo em rochas metassedimentares do greenstone belt de Crixás, Goiás. *Geol. USP. Sér. Cient.* **2010**, *10*, 118–134. (In Portuguese) [CrossRef]

27. Jost, H.; De Oliveira, A.M. Stratigraphy of the greenstone belts, Crixás region, Goiás, central Brazil. *J. South Am. Earth Sci.* **1991**, *4*, 201–214. [CrossRef]
28. Winter, J.D. *An Introduction to Igneous and Metamorphic Petrology*, 2nd ed.; Prentice Hall: New York, NY, USA, 2010.
29. Danni, J.C.M.; Ribeiro, C.C. Caracterização da seqüência vulcanossedimentar de Pilar de Goiás e Guarinos, Goiás. *SBG Congr. Brás. Geol.* **1978**, *30*, 582–596. (In Portuguese)
30. De Tarso Ferro de Oliveira Fortes, P.; Pimentel, M.M.; Santos, R.V.; Junges, S.L. Sm–Nd studies at Mina III gold deposit, Crixás greenstone belt, Central Brazil: Implications for the depositional age of the upper metasedimentary rocks and associated Au mineralization. *J. South Am. Earth Sci.* **2003**, *16*, 503–512. [CrossRef]
31. Jost, H.; Dussin, I.A.; Chemale, F., Jr.; Tassinari, C.C.G.; Junges, S. U–Pb and Sm–Nd constraints for the Paleoproterozoic age of the metasedimentary sequences of the Goiás Archean greenstone belts. In Proceedings of the 6th South American Symposium on Isotope Geology, San Carlos de Bariloche, Argentina, 13–17 April 2008.
32. Triebold, S.; Luvizotto, G.L.; Tolosana-Delgado, R.; Zack, T.; von Eynatten, H. Discrimination of TiO_2 polymorphs in sedimentary and metamorphic rocks. *Contrib. Mineral. Petrol.* **2011**, *161*, 581–596. [CrossRef]
33. Mussalam, K.; Jung, D.; Burgath, K. Textural features and chemical characteristics of chromitites in ultramafic rocks, Chalchidiki Complex (Northeastern Greece). *TMPM* **1981**, *29*, 75–101.
34. Ferrario, A.; Garuti, G. Platinum-group minerals in chromite-rich horizons of the Niquelandia Complex (Central Goias, Brazil). In *Geo-Platinum 87*; Prichard, H.M., Potts, P.J., Bowels, J.F.W., Cribb, S.J., Eds.; Springer: Berlin, Germany, 1988; pp. 261–272.
35. Kudeir, A.A.; El Haddad, M.A.; Leake, B.E. Compositional variation in chromite from the Eastern Desert, Egypt. *Mineral. Mag.* **1992**, *56*, 567–574. [CrossRef]
36. Ahmed, A.H.; Arai, S.; Attia, A.K. Petrological characteristics of podiform chromitites and associated peridotites of the Pan African Proterozoic ophiolite complexes of Egypt. *Miner. Depos.* **2001**, *36*, 72–84. [CrossRef]
37. Ahmed, A.H.; Harbi, H.M.; Habtoor, A.M. Compositional variations and tectonic settings of podiform chromitites and associated ultramafic rocks of the Neoproterozoic ophiolite at Wadi Al Hwanet, northwestern Saudi Arabia. *J. Asian Earth Sci.* **2012**, *56*, 118–134. [CrossRef]
38. Ahmed, A.H. Highly depleted harzburgite–dunite–chromitite complexes from the Neoproterozoic ophiolite, south Eastern Desert, Egypt: A possible recycled upper mantle lithosphere. *Precambrian Res.* **2013**, *233*, 173–192. [CrossRef]
39. Purvis, A.C.; Nesbitt, R.W.; Hallberg, J.A. The geology of part of the Carr Boyd Complex and its associated nickel mineralization, Western Australia. *Econ. Geol.* **1972**, *67*, 1093–1113. [CrossRef]
40. Evans, B.W.; Frost, B.R. Chome-spinel in progressive metamorphism—A preliminary analysis. *Geochim. Cosmochim. Acta* **1975**, *39*, 959–972. [CrossRef]
41. De Freitas Suita, M.T.; Strieder, A.J. Cr-spinels from Brazilian mafic–ultramafic complexes: Metamorphic modifications. *Int. Geol. Rev.* **1996**, *38*, 245–267. [CrossRef]
42. Sack, R.O.; Ghiorso, M.S. Chromian spinels as petrogenetic indicators: Thermodynamic and petrological applications. *Am. Mineral.* **1991**, *76*, 827–847.
43. Barnes, S.J. Chromite in komatiites, II. Modification during greenschist to mid-amphibolite facies metamorphism. *J. Petrol.* **2000**, *41*, 387–409. [CrossRef]
44. Tomkins, H.S.; Powell, R.; Ellis, D.J. The pressure dependence of the zirconium-in-rutile thermometer. *J. Metamorph. Geol.* **2007**, *25*, 703–713. [CrossRef]
45. Ferry, J.M.; Watson, E.B. New thermodynamic models and revised calibrations for the Ti-in-zircon and Zr-in-rutile thermometers. *Contrib. Mineral. Petrol.* **2007**, *154*, 429–437. [CrossRef]
46. Tailby, N.D.; Walker, A.M.; Berry, A.J.; Hermann, J.; Evans, K.A.; Mavrogenes, J.A.; O'Neill, H.St.C.; Rodina, I.S.; Soldatov, A.V.; Rubatto, D.; et al. Ti site occupancy in zircon. *Geochim. Cosmochim. Acta* **2011**, *75*, 905–921. [CrossRef]
47. Matveev, S.; Ballhaus, C. Role of water in the origin of podiform chromitite deposits. *Earth Planet. Sci. Lett.* **2002**, *203*, 235–243. [CrossRef]
48. Parnell, J. Titanium mobilization by hydrocarbon fluids related to sill intrusions in a sedimentary sequence, Scotland. *Ore Geol. Rev.* **2004**, *24*, 155–167. [CrossRef]

49. Arai, S.; Ishimaru, S.; Mizukami, T. Methane and propane microinclusions in olivine in titanoclinohumite-bearing dunites from the Sanbagawa high-P metamorphic belt, Japan: Hydrocarbon activity in a subduction zone and Ti mobility. *Earth Planet. Sci. Lett.* **2012**, *353–354*, 1–11. [CrossRef]
50. Seward, T.M.; Williams-Jones, A.E.; Migdisov, A. The chemistry of metal transport and deposition by ore-forming hydrothermal fluids. In *Treatise on Geochemistry*, 2nd ed.; Holland, H., Turekian, K., Eds.; Elsevier Ltd.: Oxford, UK, 2014; Volume 13, pp. 29–57.
51. Wu, Y.B.; Gao, S.; Zhang, H.F.; Yang, S.H.; Liu, X.C.; Jiao, W.F.; Liu, Y.S.; Yuan, H.L.; Gong, H.J.; He, M.C. U–Pb age, trace-element, and Hf-isotope compositions of zircon in a quartz vein from eclogite in the western Dabie Mountains: Constraints on fluid flow during early exhumation of ultra high-pressure rocks. *Am. Mineral.* **2009**, *94*, 303–312. [CrossRef]
52. Van Sijl, J.; Allan, N.L.; Davies, G.R.; van Westrenen, W. Titanium in subduction zone fluids: First insights from ab initio molecular metadynamics simulations. *Geochim. Cosmochim. Acta* **2010**, *74*, 2797–2810. [CrossRef]
53. Zhou, M.F.; Bai, W.J. Chromite deposits in China and their origin. *Miner. Depos.* **1992**, *27*, 192–199. [CrossRef]
54. Auge, T.; Johan, Z. Comparative study of chromite deposits from Troodos, Vourinos, North Oman and New Caledonia ophiolites. In *Mineral Deposits within the European Community*; Boissonnas, J., Omenetto, P., Eds.; Springer: Berlin, Germany, 1988; pp. 267–288.
55. Nakagawa, M.; Franco, H.E.A. Placer Os-Ir-Ru alloys and sulfides: Indicators of sulfur fugacity in an ophiolite? *Can. Mineral.* **1997**, *35*, 144l–1452.
56. Garuti, G.; Zaccarini, F.; Economou-Eliopoulos, M. Paragenesis and composition of laurite in chromitites of Othrys (Greece): Implication for Os-Ru fractionation in ophiolitic upper mantle of the Balkan peninsula. *Miner. Depos.* **1999**, *34*, 312–319. [CrossRef]
57. Garuti, G.; Zaccarini, F.; Moloshag, V.; Alimov, V. Platinum-Group minerals as indicator of sulfur fugacity in ophiolitic upper mantle: An example from chromitites of the Ray-Iz ultramafic complex (Polar Urals, Russia). *Can. Mineral.* **1999**, *37*, 1099–1115.
58. Kapsiotis, A.; Grammatikopoulos, T.A.; Tsikouras, B.; Hatzipanagiotou, K.; Zaccarini, F.; Garuti, G. Mineralogy, composition and PGM of chromitites from Pefki, Pindos ophiolite complex (NW Greece): Evidence for progressively elevated fAs conditions in the upper mantle sequence. *Mineral. Petrol.* **2011**, *101*, 129–150. [CrossRef]
59. Escayola, M.; Garuti, G.; Zaccarini, F.; Proenza, J.A.; Bedard, J.H.; Van Staal, C. Chromitite and platinum-group element mineralization at middle Arm Brook, central Advocate ophiolite complex, Baie Verte peninsula, Newfoundland, Canada. *Can. Mineral.* **2011**, *49*, 1523–1547. [CrossRef]
60. Prichard, H.M.; Sá, J.H.S.; Fisher, P.C. Platinum-group mineral assemblages and chromite composition in the altered and deformed Bacuri complex, Amapá, northeastern Brazil. *Can. Mineral.* **2001**, *39*, 377–396. [CrossRef]